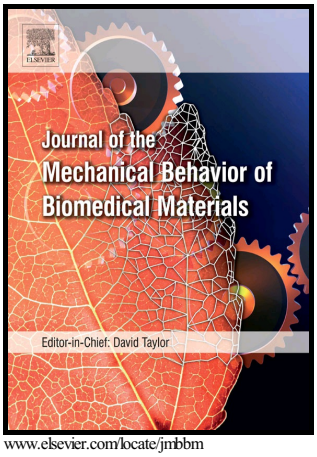

www.elsevier.com/locate/jmbbm

The cardiac torsion as a sensitive index of heart pathology: a model study

E. Cutrí, M. Serrani, P. Bagnoli, R. Fumero, M.L. Costantino

PII: S1751-6161(15)00382-3
DOI: http://dx.doi.org/10.1016/j.jmbbm.2015.10.009
Reference: JMBBM1650

To appear in: *Journal of the Mechanical Behavior of Biomedical Materials*

Received date: 9 July 2015
Revised date: 13 October 2015
Accepted date: 22 October 2015

Cite this article as: E. Cutrí, M. Serrani, P. Bagnoli, R. Fumero and M.L Costantino, The cardiac torsion as a sensitive index of heart pathology: a mode study, *Journal of the Mechanical Behavior of Biomedical Materials* http://dx.doi.org/10.1016/j.jmbbm.2015.10.009

The cardiac torsion as a sensitive index of heart pathology: a model study

E. Cutrì[a,1,*], M. Serrani[b,1], P. Bagnoli[a], R. Fumero[a], M.L. Costantino[a]

[a] *Laboratory of Biological Structure Mechanics (LaBS), Department of Chemistry, Materials and Chemical Engineering "Giulio Natta", Politecnico di Milano, Piazza Leonardo da Vinci 32, 20133, Milano, Italy*

[b] *Department of Chemical Engineering and Biotechnology, University of Cambridge Pembroke Street, Cambridge, CB2 3RA, UK*

Abstract

The torsional behaviour of the heart (*i.e.* the mutual rotation of the cardiac base and apex) was proved to be sensitive to alterations of some cardiovascular parameters, *i.e.* preload, afterload and contractility. Moreover, pathologies which affect the fibers architecture and cardiac geometry were proved to alter the cardiac torsion pattern. For these reasons, the cardiac torsion represents a sensitive index of ventricular performance. The aim of this work is to provide further insight into physiological and pathological alterations of the cardiac torsion by means of computational analyses, combining a structural model of the two ventricles with simple lumped parameter models of both the systemic and the pulmonary circulations. Starting from diagnostic images, a 3D anatomy based geometry of the two ventricles was reconstructed. The myocytes orientation in the ventricles was assigned according to literature data and the myocardium mechanical behavior was modelled by an anisotropic hyperelastic law. Both the active and the passive phases of the cardiac cycle were modelled, and different clinical conditions were simulated. The results in terms of alterations of the cardiac torsion in the presence of pathologies are in agreement

*Corresponding author

Email addresses: elena.cutri@polimi.it (E. Cutrì), ms2214@cam.ac.uk (M. Serrani), paola.bagnoli@polimi.it (P. Bagnoli), roberto.fumero@polimi.it (R. Fumero), marialaura.costantino@polimi.it (M.L. Costantino)

[1] The authors contributed equally to this work.

with experimental literature data. The use of a computational approach allowed the investigation of the stress and strain distributions in the ventricular wall as well as of the global hemodynamic parameters of the ventricle in the presence of the considered pathologies. Furthermore, the model outcomes highlight how for specific pathological conditions like the heart failure, an altered torsional pattern of the ventricles can be present, encouraging the use of the ventricular torsion in the clinical practice.

Keywords: cardiac mechanics, cardiac torsion, finite element model, myocardial infarction, hypertension

2010 MSC: 00-01, 99-00

1. Introduction

The cardiac torsion *i.e.* the mutual rotation of the cardiac base and apex, is conventionally defined as the difference between the cardiac apical and basal cross-sections rotation. A counter-clockwise rotation when viewed from the apex is conventionally assumed as positive. During initial isovolumic contraction, the apex and the base both rotate in a counter-clockwise direction [1]; during the systole the base changes direction and starts to rotate in a clockwise direction, while the apex continues to rotate counterclockwise, causing the torsional peak. This peak is then followed by a rapid untwisting of the ventricle during the isovolumic relaxation: the potential elastic energy stored in the collagen matrix and cytoskeletal proteins (titin) is released (recoil), causing the rapid untwisting [2], [3] and contributing to an active suction of blood from the atria.The cardiac torsion is due to the peculiar architecture of the heart. Several studies highlighted the presence of obliquely oriented muscle fibres whose orientation varies from a right-handed helix at the subendocardium to a left-handed helix at the subepicardium [4], [5], [6], [7]. This spiral organization seems to be fundamental in determining both the cardiac systolic and diastolic function [8]. The torsional behaviour of the heart was proved to be sensitive to the alteration of some cardiovascular parameters, *i.e.* preload, afterload and contractility.

Moreover, pathologies which affect the fibers architecture and cardiac geometry were proved to alter the cardiac torsion pattern. For these reasons, the cardiac torsion represents a sensitive index of ventricular performance [9], [10], [11], [12], [13]. The assessment of cardiac torsion as a sensitive clinical index has led to a substantial increase of the number of experimental and clinical studies aimed at quantifying this parameter. The relevant improvement of the imaging techniques in the last 20 years strongly supported this trend. Different methods have been used to measure the experimental parameters characterizing the torsional behavior (e.g. angular velocity, rotation angle); the first approaches used radiographic tracking of myocardial markers ([14], [15], [16], [17], [18], [19]), optical devices ([20], [21], [22], [23]) and two-dimensional echocardiography ([24], [25]). Lately, tissue-tagging magnetic resonance imaging (tagged MRI) has permitted to obtain non-invasive measurement of myocardial deformation in three-dimensional space and prompted investigation of left ventricle torsion ([26], [1], [27], [28], [28], [29], [30], [31], [32], [33],[34], [35], [36], [37], [38], [39], [40]). Doppler tissue imaging (DTI) has been also proposed as an efficient non-invasive method for quantifying left ventricular torsion in humans (Notomi et al. 2005-a), thanks to its higher temporal resolution with respect to MRI in the measurement of myocardial velocity. More recently, speckle tracking imaging (STI) technique, based on the appearance of speckle patterns within the tissue during two-dimensional ultrasound imaging, was used to estimate angle displacement respect to the central axis of the left ventricle ([35], [41]). Since all these non-invasive techniques are not suitable for chronic monitoring of left ventricle dynamics, a Coriolis-force based gyroscopic sensor was proposed by our research group as an alternative technique to continuously quantify in vivo Left Ventricle (LV) torsion ([42],[9],[10]). For a review on the clinical relevance of cardiac torsion, the reader is referred to [43]. In this context, a model able to reproduce the cardiac torsion pattern in both physiological and pathological conditions may provide important clinical indications. Several models have been proposed in the literature to investigate cardiac torsion using a simplified geometry [8], [44], [45], [46], [47]. More complex models were developed to inves-

tigate different aspects of heart behaviour (*i.e.*, electrical-mechanical behaviour [48], [49], [50], [51], [52], [53], [54] and [55], fluid dynamics [56], [57], [58] and mechanics [59], [60]) or to study pathological conditions [61], [62] but the cardiac torsion was only qualitatively evaluated. The aim of this work is to provide further insight into the physiological and pathological alterations of the cardiac torsion by means of computational analyses, combining a structural model of the two ventricles with simple lumped parameter models of both the systemic and the pulmonary circulations. Different clinical conditions were simulated to investigate the sensitivity of the cardiac torsion as an index of heart functioning compared to other quantities usually considered in the clinical practice, like the global cardiac haemodynamic parameters, or frequently investigated by computational studies, like the stress and strain distribution in the ventricular wall.

2. Methods

The biventricular computational model presented in this study consists of (i) an anatomy based geometrical model, (ii) a finite element (FE) model of the cardiac mechanics accounting for both the active and the passive behaviour of the myocardium and (iii) two simplified lumped parameter models representing the systemic and the pulmonary circulations.

2.1. Anatomy based geometrical model

An anatomy-based 3D geometry of the two ventricles was reconstructed by using Amira®5 (VISAGE IMAGING, Carlsbad, CA, USA) software, which allows the processing of diagnostic images. Magnetic Resonance (MRI) images of the heart of an adult healthy subject at the end of the systolic phase were provided by IRCCS San Donato, Milan, Italy. A manual segmentation of the MRI slices was performed to carefully distinguish between cardiac tissue and surrounding tissues. A smoothing process was then applied to the external and internal surfaces of the two ventricles to reduce artifacts induced by the segmen-

tation interpolation. Starting from the reconstructed surfaces, a volume was created using GAMBIT commercial code (Fluent Inc.,Lebanon, NH, USA)®. The volume was then discretized to obtain the computational mesh (Fig. 1a). The number of elements was chosen in order to obtain a good compromise between the computational costs and the results accuracy. It is worth to notice that the number of elements across the myocardial wall thickness influences the fiber orientation (*see paragraph 2.2.2*); therefore an adequate discretization along the wall thickness was chosen to properly assign the myocytes orientations. The biventricular geometry consists of 433814 tetrahedral elements, with a 437027 degrees of freedom.

2.2. FE model of cardiac mechanics

The computational model was implemented using Abaqus ®6.10 (SIMULIA, Dessault Systèmes, France) FEM modelling suite. The domain discretization was obtained using 4 node linear tetrahedral element. To handle for the incompressibility constraint, mixed formulation elements were used; this type of elements allows the treatment of the pressure stress as an independently interpolated basic solution variable, coupled to the displacement solution through the constitutive theory and the compatibility condition. This coupling is implemented by a Lagrange multiplier. The use of hybrid elements also avoids the volume locking. For detailed information on the hybrid formulation, the reader is referred to the Abaqus Documentation. The simulations were performed using quasi-static stress/displacement analyses. The non linear FE model was solved using Newton iteration algorithm.

2.2.1. Constitutive equation of the passive myocardium

In order to model the passive behaviour of the myocardial wall, the constitutive equation developed by [63] and [64] was used. Some hypotheses were formulated concerning the myocardium description: (i) the myocardium was described as an incompressible medium; (ii) the contribution of the collagen was included in the isotropic term which accounts for the matrix; (iii) all the

processes occur at a constant temperature (T=310.15K); (iv) the cardiac fibers dispersion with respect to their mean directions is assumed equal to 0 (perfectly aligned fibers). Under such hypotheses, the strain energy potential is given as:

$$\Psi = \frac{1}{2}c(\overline{I}_1 - 3) + \frac{k_1}{2k_2}\left[exp(k_2\overline{E}_i^2 - 1)\right]; \tag{1}$$

$$\overline{I}_1 = tr\overline{\mathbf{C}}; \tag{2}$$

$$\overline{I}_4 = \overline{\mathbf{C}} : \mathbf{A}; \tag{3}$$

where the first term in (1) represents the isotropic potential which accounts for the extracellular matrix contribution, while the second term represents the transversely isotropic potential due to the presence of the oriented myocytes. $\overline{I}_1$ is the first deviatoric strain invariant while the strain-like quantity $\overline{E}_i$ characterizes the deformation of the *i-th* family of fibers and, for perfectly aligned fibers, is defined as

$$\overline{E}_i = \overline{I}_{4(i,i)} - 1 \tag{4}$$

where $\overline{I_4}$ is a pseudo-invariants of $\overline{\mathbf{C}}$ (*i.e.* the distortional part of the right Cauchy-Green tensor $\overline{\mathbf{C}} = J^{-\frac{2}{3}}\mathbf{C}$) which depends on the fibers orientation, set in the reference configuration by the unit tensor $\mathbf{A}$.

The material parameters to be determined are c, namely the neo-Hookean parameter which characterizes the matrix properties, and k_1 and k_2, a stresslike and a dimensionless parameter respectively, both referred to the fibers stiffness. The estimation of those parameters was performed by fitting the physiological end diastolic volume of the right and of the left ventricle given the physiological end diastolic pressures for a healthy subject. (*see Table 1*).

2.2.2. Active contraction

To replicate the active behaviour of the myocardium, which is due to the combination of electrical, mechanical and chemical processes and results in the shortening of the sarcomers, the material parameters c and k_1 were increased

[44] during the cardiac systole (*see Table 1*) according to the profile of the force developed by a cardiomyocyte secondary to an intracellular calcium variation [65]. The variation of the fiber stiffness (k_1) was set according to the force profile and modulated to obtain the physiological systolic peak pressures (fig. 2). This simplified approach neglects all the phenomena occurring at the microscopic level but is able to reproduce the macroscopic contraction of the myocardium with a significant reduction in the model complexity and consequently in the computational demand. In this way, a simultaneous contraction of the all ventricles is considered, disregarding any spatial variation.

2.2.3. Fiber orientation

The fiber orientation was set according to literature data in both the right and the left ventricle. In particular, according to [66], the fibers orientation in the left ventricle (LV) varies from $+60°$ at the endocardium to $-60°$ at the epicardium, compared to the circumferential direction. In the right ventricle (RV) the fiber orientation ranges from $-60°$ at the epicardium to $+90°$ at the endocardium, compared to the circumferential direction. The interventricular septum was considered part of the LV [67]. This peculiar arrangement of the myocardial fibers was defined in the model by a routine *ad hoc* implemented in Matlab (The MathWorks, Inc, Natick, MA, USA). Based on a proximity criterion, the routine first categorizes each element of the mesh as part of either the left or the right ventricle. Secondly according to that classification, the fiber orientation is assigned ($-/+60°$ in the LV and $0°/90°$ in the RV). In order to ensure a smooth variation of the myocyctes direction among subsequent elements in the LV-RV transition region, the absence of discontinuities in the fiber orientation and of the quantities of interest was manually verified *a posteriori*. Particular attention was paid in analysing the apical region, where discontinuities are most likely to be found.

2.3. Lumped parameter models of the circulation

To evaluate the hemodynamic behaviour of the heart, the FE model was coupled with two lumped-parameter models (LPM) simulating a closed loop circulation, thus ensuring the blood volume conservation. In particular, one LPM simulates the systemic circulation and the other the pulmonary circulation. Each LPM comprises a resistance representing the outflow valves (the aortic valve, R_{aort}, for the systemic circulation and the pulmonary valve, R_{pulm}, for the pulmonary circulation), a constant compliance accounting for the systemic (C_{syst}) or the pulmonary (C_{pulm}) compliant blood vessels, a resistance representing the systemic (R_{psyst}) or the pulmonary (R_{ppulm}) peripheral vascular resistances, a constant compliance modelling the atrial chamber (C_{la} for the left atrium and C_{ra} for the right atrium) and a resistance representing the atrio-ventricular valves (the mitral valve, R_{mitr}, and the tricuspid valve, R_{tric}) (Fig. 3). The systemic (C_{syst}) and the pulmonary (C_{pulm}) compliance as well as the systemic (R_{psyst}) and the pulmonary (R_{ppulm}) resistances account for both the imedance of arterial and the venous pulmonary and systemic compartments, respectively. Indeed, the pressure obtained upstream to the right and left atrial compliance are equal to the physiological pressures in the inferior and superior vena cava (P_{vc}) and in the pulmonary veins (P_{pv}) respectively, just before their connection with the atria (Fig. 3). The LPM paramters used to reproduce the physiological condition are summarized in Table 2. The ventricular cavities were defined as fluid cavities by using hydrostatic elements, which allowed the coupling of the cavities pressure and volume as well as the simulation of a fluid flows from the atria to the ventricles and from the ventricles to the outflow arteries (for a detailed description of the fluid cavities implementation the reader is referred to Abaqus Documentation). Fluid properties were assumed to be the same in both cavities; any pressure gradient in the ventricles was disregarded. The fluid (blood) was modelled as an incompressible newtonian fluid with a density equal to 1060 kg/m^3. The unidirectional flow induced by the heart valves was modelled by means of diodes. In particular during the "on state" of each diode, which correspond to the valve opening, a linear pressure-flow relationship

was prescribed to the valve, while during the "off state", corresponding to the valve closure, blood flow is prescribed to zero, thus preventing backflows.

2.4. Simulation conditions

Appropriate kinematic boundary conditions were applied to the ventricular model to reproduce the effect of the surrounding tissues on in vivo heart movements and, particularly, on the ventricular torsion. Specifically, to replicate the effect of these structures without directly constraining any ventricular region, a deformable constraint was implemented and kinematically coupled to the ventricles, at the valvular plane. The deformable constraint consists of a linear elastic planar ring connected at the ventricular base; the mechanical parameters (Young's modulus=0.2 MPa; Poisson's ratio=0.35) and diameter (d=400 mm) of the ring were chosen to reproduce physiologic values of the ventricular base rotation in the healthy case. Any longitudinal displacement of the constraint plane were prevented, while rigid motions of the structure were avoided by fixing the external nodes of the ring (namely, the external circumference) in all the directions. This solution serves the purpose to reduce the effect of the constraint on the cardiac base. To simulate the whole cardiac cycle, two steps were implemented. The first step reproduces the diastole (physiological diastole duration 0.5 s) while the second step reproduces the subsequent systole (physiological systole duration 0.4 s) for a total cardiac cycle time of 0.9 s (frequency = 70 bpm). The model was used to simulate the physiological condition and some of the most widespread cardiac diseases. In particular, systemic hypertension (SYST-HYP) was simulated by increasing the R_{psyst} in the LPN from 25 $mmHg \cdot L/min$ to 35 $mmHg \cdot L/min$ while the mitral valve regurgitation (MVR) was obtained by modifying the "off state" of the diode using a linear pressure-flow relationship to allow the blackflow. Myocardial infarction at the interventricular septum (SEP-INF) and at the LV free wall (FW-INF) were obtained by decreasing the contractility (*i.e*, reduction of the contractility of the 50% with respect to the physiological case) of the correspondent regions of myocardial wall. The locations of the infarcted regions both for the SEP-INF

and the FW-INF are illustrated in figure 4. In both cases, the portion of the LV wall subjected to the reduction of the contractility corresponds to the 20% of the LV wall mass. For MVR, SEP-INF and FW-INF, the LPM parameters are assumed as for the physiological condition (Table 2). To reach a converged limit cycle of the LPM of both the systemic and the pulmonary circulation, ten cardiac cycles were performed for all the simulation conditions; a difference of the ventricles pressures lower than 5% between two subsequent cardiac cycles was considered as a reliable indicator of the system convergence.

2.5. Quantities of interest

The ventricular torsion during the cardiac cycle was measured as the difference in the angular rotation of each analyzed ventricular cross-sections with respect to the basal region (Fig. 1b). Further, to investigate the regional variation of the LV torsion, this parameter was evaluated in different locations of the LV free wall (Fig. 1c): the LV-FW, the LV-FW1 (located in the posterior portion of the left ventricle) and LV-FW2 (located in the anterior portion of the left ventricle). The Cauchy stress in the fiber direction during the systolic and the diastolic phase was measured along the myocardial wall. In particular, for a mid-longitudinal cross section three different locations were considered *i.e.* the LV and RV free walls and the interventricular septum (Fig. 1c). Further, the time profile of the myocardial strain was measured along the longitudinal, circumferential and radial direction in a point located in a mid-longitudinal cross section of the LV free wall. The circumferential-radial (CR) and circumferential-longitudinal (CL) shear strains were also calculated at two different location of the left ventricular wall (namely, at the ventricular base and apex, in the free wall). Indeed, both shear strains are strictly related with ventricular torsion [68],[69].

3. Results and Discussion

In this section the results of the simulations are presented and discussed for both the physiological and the pathological cases. First, the results of the

physiological model are reported and compared to available literature data. Secondly, the results of the pathological conditions are presented and compared with the physiological case to show any alteration induced by the simulated pathologies. Lastly, the pathological simulation results are compared against the available literature data.

3.1. Physiological condition

The pressure volume loops for the RV (blue) and the LV (red) under physiological condition are shown in figure 5. The physiological values of systolic peak pressures (SPP), end diastolic volume (EDV) and stroke volume (SV) for the RV and LV are reported in table 3. The LV shows higher SPP and EDV with respect to the RV (136.9 mmHG and 114.6 mL versus 49.7 mmHg and 106.5 mL) but a slighlty smaller SV (-1%). The physiological pressure profiles during the normalized cardiac cycle of the RV, the LV, the left atrium (LA), the right atrium (RA), the aorta and the pulmonary artery (PULM) are shown in figure 6. The Cauchy stress in the fiber direction was evaluated in the mid-longitudinal cross section of the ventricle. In particular, the stress pattern was calculated across the myocardial thickness in different regions: the LV and RV free wall and the intraventricular septum (*see fig. (1c)*). The stress patterns for these three regions in the physiological case are reported in figure 7 at the end diastole and systolic peak condition. In the LV free wall (PHYS-LV) and in the intraventricular septum (PHYS-SEP), both during diastole and systole, fiber stress was higher near the endocardial region than in the epicardial region (49 KPa at the 35% of the myocardial thickness and 41 KPa at the 23% of the myocardial thickness, respectively). In the RV free wall (PHYS-RV), the maximum tensile fiber stress (14 KPa) was found at 50% of the myocardial thickness both during diastole and systole. These different behaviour of the ventricular regions can be explained because of the myocytes orientation. Indeed, while in the LV and intraventricular septum the fiber orientation ranges from $+60^\circ$ at the endocardium to -60° at the epicardium, compared to the circumferential direction, in the right ventricle it varies from -60° at the epicardium to $+90^\circ$

at the endocardium. In all these regions, stresses in the fiber direction were higher during systole than during diastole due to cardiomyocytes contraction. It is worth to notice that the stress distributions in systole and in diastole show nearly the same trend, even if characterized by different values. Thus, the simplified mechanism here proposed to simulate the myofiber contraction allows to replicate the Frank-Starling law: the higher the myocytes stress and strain in diastole, the stronger is the contractile force the myocytes are able to develop during systole. The time profile of the myocardial strains was also measured in a point located in a middle section of the left ventricle long axis (Fig. 8); for a correct comparison of the calculated and experimental strains, the circumferential, radial and longitudinal strains were considered. In fact, even if in the physiological case the principal strain directions are pretty close to the circumferential, radial and longitudinal one, a different orientation of the principal strains was observed in case of pathology in experimental works [70].

For the physiological case, LV torsion at different cross sections along the LV long axis is reported for FW in figure 10. As expected, the cardiac torsion is higher at the ventricular apex (22°) while it decreases when reaching the cardiac base (2°) [71]. The cardiac torsion peak occurs during the systolic phase since it is determined by the fiber contraction. The torsion profile in different regions (fig. (1c)) of the LV is shown in figure 11. The cardiac torsion is higher in the LV-FW (22°) and LV-FW1 (21°) than in the LV-FW2 (16°). The first two regions are located in the antero-lateral portion of the LV while the FW2 is positioned in the posterior wall.

3.2. Comparison with literature data

According to the time tracings showed in figure (6) and the data reported in table 3, the physiological hemodynamic results are consistent with in vivo literature data of healthy subjects [72]. The myofiber stress distribution in the ventricular wall highlighted higher stress values in the midwall where the fiber are directed more circumferentially. This pattern is in agreement with the literature ([73]) and the peak stress in both the systolic and diastolic phase are

within the range of other works ([73], [74], [75], [8], [48]). However, the stress variation across the wall, especially in the left ventricle, seems to be bigger than the physiologic one. This high stress variation coul be explained due to the choice of a literature myocytes arrangement instead of a patient-specific one. In fact, the myofiber stress distribution in the ventricular wall strongly depends on the fibers orientation. The influence of myocytes orientation on wall mechanics has been demonstrated in several literature studies, and different hypotheses about the mechanisms underlying the peculiar cardiac fibers arrangement have been made ([76], [77], [78], [25], [79], [80]). Hence, even if the variation of fibres orientation among different individuals has proven to be small ([81]), the addition of a patient-specific tissue architecture measured for example by cardiac DTI could improve the accuracy of the results. The comparison of myofiber strains with literature data (fig. (8)) showed an overall agreement of the strain pattern provided by the model and the experimental data [82]. Nevertheless, the model circumferential strain was higher than the literature one during systole, while the opposite trend was observed for the radial direction. However, literature data [82], [83] showed a wide variability of the absolute values of the strain while the time profile is generally confirmed.The CR shear strain, which is related to the transmural difference of the cardiac rotation, exhibits a different pattern between the apex and the base (fig.(9)). This particular feature of ventricular kinematics has been confirmed by previous experimental works [84, 69]. A general agreement between the model results in terms of CL shear strain, which increases from the apex to the base, and literature experimental findings was also found [69]. The maximum values of the calculated shear strains are in good agreement with the aforementioned experimental literature works. Another important index to evaluate the cardiac performances is the cavity to wall volume ratio. In fact, this index has proven to be the most important geometric parameter in linking the ventricular heamodynamic variables (cavity pressure and volume) with the myofiber mechanics variables (stress and strain) ([85], [86]). Typical values of this index range among 0.15 and 0.7 ([85]); in the physiological model, the cavity to wall ratio varies between 0.3 and 0.61 during

the cardiac cycle, in agreement with literature findings. Finally, the physiological torsion pattern predicted from the model is in agreement with experimental literature measurements as well as the torsion peak values [87], [36], [35], [28] and [88]. A greater variation of the torsion is observed from the apex to the mid point than from the mid point to the base, as previously reported by [29] (section 4, fig. 10. The differences observed in the torsional behaviour of different regions of the LV wall (namely LV-FW, LV-FW1 in the antero-lateral portion and LV-FW2 in the posterior portion) are consistent with literature findings. Indeed, [29] and [43] observed a lower torsion in the posterior/ postero-lateral than the anterior/antero-lateral regions of the LV.

3.3. Pathological condition

In the next subsections, the results of the pathological consitions are presented. For the sake of clarity, the results of the pathological conditions and their comparison to the physiological case are grouped in: (i) global hemodynamic results (*i.e.*, pressure profile and pressure-volume loop of the two ventricles); (ii) local mechanics (*i.e.*, stress and strain distributions evaluated at the LV free wall, RV free wall and interventricular septum); (iii) cardiac torsion profiles during the cardiac cycle evaluated at different sections of the LV (*see paragraph 2.4*). The results obtained from simulations of pathological conditions are compared and discussed with available literature data.

3.3.1. Global hemodynamic results

The comparison among the PV loops in the physiological case and the investigated pathological conditions is summarized in figure 12. In case of systemic hypertension (SYS-HYP) (fig. 12A) the LV systolic peak pressure is higher (+12%) while the LV stroke volume is lower (−14%) than the physiological case. As a consequence, the RV end diastolic volume decreases compared to the physiological condition (−8%). By comparing physiological case to MVR condition (fig. 12B), the absence of isovolumetric phases in the LV is observed in the MVR due to the backflow through the mitral valve from the LV to the

LA. The investigation of the myocardial infarction in the intraventicular septum (fig. 12C) and in the LV free wall highlights a slightly decreased LV systolic peak pressure (-2% and -4%, respectively) while the EF decreases by -4% in FW-INF and -8% in SEP-INF.

3.3.2. Local mechanics

Myofiber stresses. For all the investigated pathological conditions, the Cauchy stress in the fiber direction was evaluated across the wall thickness in three different regions of the myocardium (*see fig. 1c*); these stresses are shown in figure 13 compared to the physiological case. In all the pathological conditions, the stress profile within the myocardial wall is preserved, with the same location of the peak values for all the three regions. The stress patterns during the systole at the LV free wall and at the intraventricular septum highlight higher stress values for the HYP, SEP-INF and FW-INF with respect to the physiological case, while the LV fibers stress under MVR is lower. These findings can be due to the increase in systolic peak pressure in HYP and to a lower contractility of a portion of the myocardium in FW-INF and SEP-INF, both phenomena leading to a general increase in myofiber stress. On the contrary, the MVR condition leads to a decrease of the LV pressure due to the backflow towards the LA during systole. By comparing the two myocardial infarction conditions, at the LV free wall higher stresses are observed for the FW-INF while the two conditions lead to quite similar results in the intraventricular septum. The comparison among the different pathologies in terms of stress profile is preserved during the diastole (the graphs are not shown for sake of brevity) with the exception of the MVR, where higher stresses at the LV free wall are observed during the ventricular filling phase. Indeed, the end diastolic volume of the LV increases in the MVR condition due to the increased atrial pressure with respect to the physiological case.

Myofiber strains. The strain profile in the longitudinal, circumferential and radial direction for the pathological conditions is reported in figure 14 compared to the physiological case. A general decrease of the longitudinal strain was ob-

served for all the pathological conditions with respect to the physiological case. The comparison of the pathological circumferential strains to the physiological case showed an increase in the MVR case (+23%) while for the FW-INF and HYP a decrease was observed (−14% and −12%, respectively). The same trend was observed in the radial strain: +7% in MVR, −20% in HYP, −19% in FW-INF and −8% in SEP-INF.

3.3.3. Cardiac torsion

For all the considered cases, we report the cardiac torsion within the cardiac cycle measured as the difference of the angular rotation of apical section with respect to the basal region. The comparison of the physiological LV torsion with the pathological conditions is summarized in figure 15. The comparison highlighted a slight decrease in the torsion peak value was observed in the HYP with respect to the PHYS condition. The cardiac torsion also significant decreases (−27%) in FW-INF. Concerning the MVR case, a lower diastolic recoil rate was found. An interesting result of the performed simulations is the different cardiac torsion trends showed by the two myocardial infarction conditions (FW-INF and SEP-INF). With respect to the physiological conditions, an increase in the torsion peak value is highlighted in the FW-INF (+27%) while the opposite trend occurs in the SEP-INF (−27%). A possible explanation of this opposite behaviour may be the different pressure gradient across the myocardial wall at the interventricular septum and at the free wall. Indeed, even if the the same contractily decrease was imposed, the interventricular septum motion is also constricted by the right ventricular cavity pressure which may also contribute to the reduction of the cardiac torsion.

3.3.4. Comparison with literature data

The local mechanics results obtained from pathological simulations showed a good agreement with literature data. In particular, [89] evaluated the LV strains in patients suffering from MV regurgitation with control group before and after mitral valve repair by means of speckle tracking analysis. A general

increase in the LV strain was found in patients with MVR than in normal control individuals; the same trend was observed in our model as confirmed by figure 14 where an increase of the radial and circumferential strains in MVR with respect to PHYS condition is found. Concerning the stress distribution, we observed a reduction in the LV stresses in MVR. This finding is corroborated by a study conducted by [90] in 1432 patients with MVR recorded in the transthoracic echocardiography where lower end systolic stresses were found in patients with 1st and 2nd degrees of MVR with respect to the normal controls. With reference to the HYP condition, higher stresses values were found for all the considered locations while the opposite trend is observed for the radial, circumferential and longitudianal strains with respect to the PHYS condition. The former results are confirmed by [91], who proposed a finite element model of the LV coupled to system circulation model to evaluate the effect of different grades of hypertension on wall mechanics. The comparison of results obtained from the simulation of the hypertension condition and those from the physiological case showed an increase of +21% in the average fiber stress levels in mild hypertensive case and of +36% in the moderate hypertension case. Concerning the latter results, the same behaviour was assessed by [92] who investigated the LV strain in in patients with systemic hypertension and preserved LV systolic function. The longitudinal strains in patient with systemic hypertension were attenuated in comparison with normal controls as well as circumferential strain.

The decrease in the torsion peak value observed in the HYP with respect to the PHYS condition is confirmed by Macgowan and colleagues in 1996 [93] that used Magnetic Resonance Imaging tagging to evaluate cardiac torsion in 10 canine hearts with altered afterload. In a study from [37] the alteration of cardiac torsion is evaluated when the afterload is increased. A reduction of the cardiac torsion of the 50% was also observed if the ESV increases from 14.5 mL to 21.5 mL. In our cases the same trend is observed with smaller difference from HYP to PHYS due to the lower ESV variation (from 58 mL in PHYS to 63 mL in HYP). Other literature studies investigated the effect of hypertension on cardiac torsions [37]. Nevertheless, those studies are not comparable with

the results here presented since in the present work only acute pathological changes are taken into account, disregarding any long-term effect which may occur with a persistent pathological condition. Different literature studies [94], [21] and [22] assessed a decrease in the torsion peak in case of acute myocardial infarction, thus confirming model results in case of SEP-INF. Concerning the MVR case, the presence of a lower diastolic recoil rate observed in the MVR torsion is corroborated by literature findings [18]. Further, [95] evaluated the modification of cardiac torsion in patient suffering from chronic mitral valve regurgitation; delay and slowing of the LV untwisting were found. The authors suggested the use of the torsion parameter to asses desease severity and early signs of ventricular dysfunction.

4. Limitations

All the aforementioned results are based on the computational biventricular model, which is subjected to some limitations addressed below. Although the methodologhy used to model the fibers contraction well reproduces the macroscopic active behavior of the myocardium, more accurate predictions could be achieved by coupling the FE model to an electrophysiology model accounting for the electrical phenomena occurring at lower spatial scale. A fibre orientation consistent with literature physiological data was assumed. Even though, the fibre orientation range in physiological conditions was proved to have a low inter-patients difference, it may be significantly altered in pathological conditions. For this reason, this approximation in pathological condition may lead to incorrect estimation of the myocardial anisotropy. However, the routine *ad hoc* implemeted in Matlab to assign the fiber orientation easily allows the definition of different fiber distributions thus enabling the modelling of patient specific (physiological or pathological) fiber architecture, if specific data are provided. The simulations were performed using quasi static stress/displacement analysis thus neglecting the system inertia. The use of static load steps was chosen since preliminary tests performed under dynamic conditions showed unrealistic

numerical oscillations of the kinematic outcomes, probably due to the absence of the fluid modelling. However, the preliminary dynamic analyses showed that the kinematic energy is negligible if compared to the strain energy of the system, thus justifying the use of the quasi- static approach. In this work, the contribution of the residual stresses has been neglected. This assumption may lead to an overestimation of the predicted endocardial stress. The literature reports only few data regarding the quantification and the distribution of the residual stresses in the left ventricle. In fact, some works report a small influence of the residual stresses and strains on the end-diastolic mechanics of the left ventricle ([96], [97]) but the role in the systolic phase is still not clarified. However, to completely investigate the residual stresses and determine the most suitable constitutive law for the cardiac tissue, additional experimental data would be required. To the best of our knowledge, investigation on the residual stress of the RV has not been performed yet. In conclusion, due to the lack of experimental data and the complexity of residual stress modelling during the systolic phase, and relying on the literature data, we decided not to account for these stresses assuming that this simplification can be acceptable for the purpose of our paper. The myocardium was modelled as a transversely isotropic medium. This assumption is surely a simplification regarding the tissue behaviour, which is actually orthotropic as highlighted by several literature studies ([98], [99], [100]). The modelling of the extracellular matrix and its complex architecture would give a more accurate description of the material mechanics, allowing a detailed analysis of the shear strains and wall thickening in different pathological conditions. Nevertheless, the main characteristics of the cardiac tissue mechanics can be adequately described by the proposed constitutive law. In fact, all the quantities of interest for the aim of the present study where well reproduced by the model and comparable with experimental data. To properly define the kinematic boundary conditions, a realistic modeling of all the structures surrounding the ventricles would be necessary; since this is beyond the aim of this study, a simplified approach consisting in the implementation of a deformable constraint aimed only at the simulation of the effect of the presence of these

structures on the ventricular kinematics was adopted. This choice affects the calculated displacements, especially in terms of rotation of the ventricular base. However, the constraint characteristics have been carefully chosen to obtain physiologic values of the base rotation in the healthy case, ensuring more realistic results than what would be obtained by directly constraining regions of the ventricles, as usually found in the literature (e.g. [101][61][82]). Also, the torsion is mainly due to the rotation of the ventricular apex, which is not influenced by the presence of such a constraint. Lastly, this study is aimed at investigating the effectiveness of cardiac torsion as an indicator of heart pathologies by comparing its alteration with respect to the physiological condition; such a comparison is not affected by the kinematical constraint used. Finally, eventhough the coupling of the FE model with the lumped-parameters models simulating the systemic and pulmonary circulations allowed the evaluation of the myocardial response under physiological and pathological conditions, in the fluid flow modeling presented in this work the fluid inertia was neglected. Fluid-structure models could better describe the interactions between blood flow and the deforming vascular structure, as well as the energy based mechanism driving the transport processes; however it is well known how such models lead to higher complexity and computational costs.

5. Conclusions

In this study a finite element model of the two heart ventricles was developed and coupled to two LPMs of the systemic and pulmonary circulations. To correctly reproduce the myocardial mechanical behaviour, a hyperelastic constitutive law was used and the presence of fiber orientation was taken into account. The active behaviour of the myocardium was modelled using a simple mechanism that allows the reproduction of the macroscopic heart contraction. This choice allowed also to reduce the complexity of the model definition since it does not requires the modelling of lower scale phenomena. The passive and active material properties were determined to match the literature data for end

diastolic volume and systolic peak pressure, respectively. LPM parameters were estimated to reproduce the PV loops. The 3D FE model was then coupled to LPMs obtaining a closed-loop circulation model to simulate complete cardiac cycles. Physiological and pathological conditions were simulated. As shown in the results and discussion section, both physiological and pathological simulation outcomes are in general agreement with available literature data. The model can be used to predict global parameters as well as local function of the heart, some of which cannot be directly measured in the patient. The model here presented can also be used to investigate further pathologies such as mitral or aortic vale stenosis, pulmonary hypertension and myocardial infarction in different portion of the cardiac wall by properly altering either the LPM parameter or the contractility of the myocardium. Concerning the cardiac torsion, the comparison of the physiological condition with the pathological cases gives rise to interesting speculations. The cardiac torsion pattern in the pathological cases is shown to deviate from the physiological condition, thus demostrating the efficacy of such a parameter to discriminate pathological events. It is worth to notice that in case of both SEP-INF and FW-INF, only a slightly decreased LV systolic peak pressure was found compared to the physiological (-2% and -4%, respectively) and the EF slightly decreases by -4% in FW-INF and -8% in SEP-INF. On the contrary, the evaluation of the cardiac torsion in these two pathological cases showed a remarkable difference with respect to the physiological case (increase of the torsion peak value of the ($+27\%$) in the FW-INF and decrease of the (-27%) in the SEP-INF). This comparison may suggest the ability of the cardiac torsion parameter to reveal even moderate pathological conditions which are not detected from the analysis of the classical hemodynamic parameters. Moreover, the opposite trends found in the cardiac torsion pattern in the FW-INF and in the SEP-INF conditions, which may results from the different pressure gradient across the myocardial wall at the interventricular septum and at the free wall, further indicate the reliability of the cardiac torsion as a sensitive index of the cardiac performance. So, the evaluation of the cardiac torsion in addition to classical clinical indices may provide important

indication on the heart performances and may consequently represent a valuable tool in the clinical practice. Computational models are often used to assist the surgeons in deciding the best surgical treatment to be performed thanks to their ability to simulate different postoperative scenarios. In this context, the analysis of cardiac torsion coupled with the classical mechanical parameters (stress, strain, etc.) may provide the clinician a more complete frame of the outcomes of different possible surgical treatments. To conclude, this model presents the cardiac torsion as a new metric for cardiac performance and could be a starting point for its systematic evaluation in different pathologic conditions.

References

[1] C. H. Lorenz, J. S. Pastorek, J. M. Bundy, Delineation of normal human left ventricular twist throughout systole by tagged cine magnetic resonance imaging, Journal of Cardiovascular Magnetic Resonance 2 (2) (2000) 97–108, cited By :104.

[2] F. E. Rademakers, W. J. Rogers, W. H. Guier, G. M. Hutchins, C. O. Siu, M. L. Weisfeldt, J. L. Weiss, E. P. Shapiro, Relation of regional cross-fiber shortening to wall thickening in the intact heart: Three-dimensional strain analysis by nmr tagging, Circulation 89 (3) (1994) 1174–1182, cited By (since 1996):190.

[3] Y. Notomi, M. G. Martin-Miklovic, S. J. Oryszak, T. Shiota, D. Deserranno, Z. B. Popovic, M. J. Garcia, N. L. Greenberg, J. D. Thomas, Enhanced ventricular untwisting during exercise: A mechanistic manifestation of elastic recoil described by doppler tissue imaging, Circulation 113 (21) (2006) 2524–2533, cited By (since 1996):158.

[4] F. Torrent-Guasp, M. J. Kocica, A. F. Corno, M. Komeda, F. Carreras-Costa, A. Flotats, J. Cosin-Aguillar, H. Wen, Towards new understanding of the heart structure and function, European Journal of Cardio-thoracic Surgery 27 (2) (2005) 191–201, cited By (since 1996):92.

[5] F. Torrent-Guasp, M. Ballester, G. D. Buckberg, F. Carreras, A. Flotats, I. Carri, A. Ferreira, L. E. Samuels, J. Narula, Spatial orientation of the ventricular muscle band: Physiologic contribution and surgical implications, Journal of Thoracic and Cardiovascular Surgery 122 (2) (2001) 389–392, cited By (since 1996):124.

[6] F. Torrent-Guasp, G. D. Buckberg, C. Clemente, J. L. Cox, H. C. Coghlan, M. Gharib, The structure and function of the helical heart and its buttress wrapping. i. the normal macroscopic structure of the heart, Seminars in thoracic and cardiovascular surgery 13 (4) (2001) 301–319, cited By (since 1996):102.

[7] F. Torrent-Guasp, M. J. Kocica, A. Corno, M. Komeda, J. Cox, A. Flotats, M. Ballester-Rodes, F. Carreras-Costa, Systolic ventricular filling, European Journal of Cardio-thoracic Surgery 25 (3) (2004) 376–386, cited By (since 1996):64.

[8] T. Arts, R. S. Reneman, P. C. Veenstra, A model of the mechanics of the left ventricle, Annals of Biomedical Engineering 7 (3-4) (1979) 299–318, cited By (since 1996):110.

[9] E. Marcelli, L. Cercenelli, M. Parlapiano, R. Fumero, P. Bagnoli, M. L. Costantino, G. Plicchi, Effect of right ventricular pacing on cardiac apex rotation assessed by a gyroscopic sensor, ASAIO Journal 53 (3) (2007) 304–309.

[10] E. Marcelli, L. Cercenelli, M. Musaico, P. Bagnoli, M. L. Costantino, R. Fumero, G. Plicchi, Assessment of cardiac rotation by means of gyroscopic sensors, in: Computers in Cardiology, Vol. 35, 2008, pp. 389–392, cited By (since 1996):2.

[11] I. K. Rssel, M. J. W. Gtte, J. G. Bronzwaer, P. Knaapen, W. J. Paulus, A. C. van Rossum, Left ventricular torsion. an expanding role in the analysis of myocardial dysfunction, JACC: Cardiovascular Imaging 2 (5) (2009) 648–655, cited By (since 1996):44.

[12] B. T. Esch, D. E. R. Warburton, Left ventricular torsion and recoil: Implications for exercise performance and cardiovascular disease, Journal of applied physiology 106 (2) (2009) 362–369, cited By (since 1996):17.

[13] E. Cutrì, P. Bagnoli, E. Marcelli, F. Biondi, L. Cercenelli, M. L. Costantino, G. Plicchi, R. Fumero, A mechanical simulator of cardiac wall kinematics, ASAIO Journal 56 (3) (2010) 164–171, cited By :1.

[14] N. B. I. Jr., D. E. Hansen, G. T. D. II, E. B. Stinson, E. L. Alderman, D. C. Miller, Relation between longitudinal, circumferential, and oblique shortening and torsional deformation in the left ventricle of the transplanted human heart, Circulation research 64 (5) (1989) 915–927, cited By :165.

[15] D. E. Hansen, G. T. D. II, E. L. Alderman, E. B. Stinson, J. C. Baldwin, D. C. Miller, Effect of acute human cardiac allograft rejection on left ventricular systolic torsion and diastolic recoil measured by intramyocardial markers, Circulation 76 (5) (1987) 998–1008, cited By :76.

[16] D. E. Hansen, G. T. D. II, E. L. Alderman, N. B. Ingels, E. B. Stinson, D. C. Miller, Effect of volume loading, pressure loading, and inotropic stimulation on left ventricular torsion in humans, Circulation 83 (4) (1991) 1315–1326, cited By :98.

[17] M. R. Moon, N. B. I. Jr., G. T. D. II, E. B. Stinson, D. E. Hansen, D. C. Miller, Alterations in left ventricular twist mechanics with inotropic stimulation and volume loading in human subjects, Circulation 89 (1) (1994) 142–150, cited By :136.

[18] F. A. Tibayan, K. L. Yun, D. T. M. Lai, T. A. Timek, G. T. Daughters, N. B. Ingels, D. C. Miller, Torsion dynamics in the evolution from acute to chronic mitral regurgitation, Journal of Heart Valve Disease 11 (1) (2002) 39–46.

[19] F. A. Tibayan, D. T. M. Lai, T. A. Timek, P. Dagum, D. Liang, G. T. Daughters, N. B. Ingels, D. C. Miller, Alterations in left ventricular torsion in tachycardia-induced dilated cardiomyopathy, Journal of Thoracic and Cardiovascular Surgery 124 (1) (2002) 43–49, cited By :65.

[20] C. A. G. Kroeker, H. E. D. J. T. Keurs, M. L. Knudtson, J. V. Tyberg, R. Beyar, An optical device to measure the dynamics of apex rotation of the left ventricle, American Journal of Physiology - Heart and Circulatory Physiology 265 (4 34-4) (1993) H1444–H1449, cited By :48.

[21] C. A. G. Kroeker, J. V. Tyberg, R. Beyar, Effects of ischemia on left ventricular apex rotation an experimental study in anesthetized dogs, Circulation 92 (12) (1995) 3539–3548.

[22] M. L. Knudtson, P. D. Galbraith, K. L. Hildebrand, J. V. Tyberg, R. Beyar, Dynamics of left ventricular apex rotation during angioplasty: A sensitive index of ischemic dysfunction, Circulation 96 (3) (1997) 801–808.

[23] N. B. I. Jr., G. T. D. II, E. B. Stinson, E. L. Alderman, Measurement of midwall myocardial dynamics in intact man by radiography of surgically implanted markers, Circulation 52 (5) (1975) 859–867, cited By :115.

[24] M. J. Mirro, E. W. Rogers, A. E. Weyman, H. Feigenbaum, Angular displacement of the papillary muscles during the cardiac cycle, Circulation 60 (2) (1979) 327–333, cited By :39.

[25] T. Arts, S. Meerbaum, R. S. Reneman, E. Corday, Torsion of the left ventricle during the ejection phase in the intact dog, Cardiovascular research 18 (3) (1984) 183–193, cited By :86.

[26] C. C. Moore, C. H. Lugo-Olivieri, E. R. McVeigh, E. A. Zerhouni, Three-dimensional systolic strain patterns in the normal human left ventricle: Characterization with tagged mr imaging, Radiology 214 (2) (2000) 453–466, cited By :252.

[27] D. C. Miller, Alterations in left ventricular diastolic twist mechanics during acute human cardiac allograft rejection, Circulation 83 (3) (1991) 962–973, cited By :92.

[28] J. J. W. Sandstede, T. Johnson, K. Harre, M. Beer, S. Hofmann, T. Pabst, W. Kenn, W. Voelker, S. Neubauer, D. Hahn, Cardiac systolic rotation and contraction before and after valve replacement for aortic stenosis: A myocardial tagging study using mr imaging, American Journal of Roentgenology 178 (4) (2002) 953–958, cited By (since 1996):59.

[29] M. B. Buchalter, F. E. Rademakers, J. L. Weiss, W. J. Rogers, M. L. Weisfeldt, E. P. Shapiro, Rotational deformation of the canine left ventricle measured by magnetic resonance tagging: effects of catecholamines, ischaemia, and pacing, Cardiovascular research 28 (5) (1994) 629–635, cited By :109.

[30] S. E. Maier, S. E. Fischer, G. C. McKinnon, O. M. Hess, H. P. Krayenbuehl, P. Boesiger, Evaluation of left ventricular segmental wall motion in hypertrophic cardiomyopathy with myocardial tagging, Circulation 86 (6) (1992) 1919–1928, cited By :129.

[31] S. J. Dong, P. S. Hees, C. O. Siu, J. L. Weiss, E. P. Shapiro, Mri assessment of lv relaxation by untwisting rate: A new isovolumic phase measure of t, American Journal of Physiology - Heart and Circulatory Physiology 281 (5 50-5) (2001) H2002–H2009, cited By :153.

[32] M. B. Buchalter, J. L. Weiss, W. J. Rogers, E. A. Zerhouni, M. L. Weisfeldt, R. Beyar, E. P. Shapiro, Noninvasive quantification of left ventricular rotational deformation in normal humans using magnetic resonance imaging myocardial tagging, Circulation 81 (4) (1990) 1236–1244, cited By :244.

[33] R. M. Setser, J. M. Kasper, M. L. Lieber, R. C. Starling, P. M. McCarthy, R. D. White, Persistent abnormal left ventricular systolic torsion in dilated

cardiomyopathy after partial left ventriculectomy, Journal of Thoracic and Cardiovascular Surgery 126 (1) (2003) 48–55, cited By :43.

[34] E. Nagel, M. Stuber, M. Lakatos, M. B. Scheidegger, P. Boesiger, O. M. Hess, Cardiac rotation and relaxation after anterolateral myocardial infarction, Coronary artery disease 11 (3) (2000) 261–267, cited By :73.

[35] Y. Notomi, R. M. Setser, T. Shiota, M. G. Martin-Miklovic, J. A. Weaver, Z. B. Popovic, H. Yamada, N. L. Greenberg, R. D. White, J. D. Thomas, Assessment of left ventricular torsional deformation by doppler tissue imaging: Validation study with tagged magnetic resonance imaging, Circulation 111 (9) (2005) 1141–1147, cited By (since 1996):148.

[36] E. Fuchs, M. F. Mller, H. Oswald, H. Thny, P. Mohacsi, O. M. Hess, Cardiac rotation and relaxation in patients with chronic heart failure, European Journal of Heart Failure 6 (6) (2004) 715–722, cited By (since 1996):50.

[37] S. J. Dong, P. S. Hees, W. M. Huang, S. A. B. Jr., J. L. Weiss, E. P. Shapiro, Independent effects of preload, afterload, and contractility on left ventricular torsion, American Journal of Physiology - Heart and Circulatory Physiology 277 (3 46-3) (1999) H1053–H1060, cited By :118.

[38] J. Chung, P. Abraszewski, X. Yu, W. Liu, A. J. Krainik, M. Ashford, S. D. Caruthers, J. B. McGill, S. A. Wickline, Paradoxical increase in ventricular torsion and systolic torsion rate in type i diabetic patients under tight glycemic control, Journal of the American College of Cardiology 47 (2) (2006) 384–390, cited By :72.

[39] M. J. W. Gotte, T. Germans, I. K. Russel, J. J. M. Zwanenburg, J. T. Marcus, A. C. van Rossum, D. J. van Veldhuisen, Myocardial strain and torsion quantified by cardiovascular magnetic resonance tissue tagging. studies in normal and impaired left ventricular function, Journal of the American College of Cardiology 48 (10) (2006) 2002–2011, cited By :99.

[40] J. J. M. Zwanenburg, J. P. A. Kuijer, J. T. Marcus, R. M. Heethaar, Steady-state free precession with myocardial tagging: Cspamm in a single breathhold, Magnetic Resonance in Medicine 49 (4) (2003) 722–730, cited By :51.

[41] T. Helle-Valle, J. Crosby, T. Edvardsen, E. Lyseggen, B. H. Amundsen, H. J. Smith, B. D. Rosen, J. A. Lima, H. Torp, H. Ihlen, O. A. Smiseth, New noninvasive method for assessment of left ventricular rotation: speckle tracking echocardiography., Circulation 112 (20) (2005) 3149–3156, cited By :455.

[42] E. Marcelli, G. Plicchi, L. Cercenelli, F. Bortolami, First experimental evaluation of cardiac apex rotation with an epicardial coriolis force sensor, ASAIO Journal 51 (6) (2005) 696–701, cited By :11.

[43] S. M. Shaw, D. J. Fox, S. G. Williams, The development of left ventricular torsion and its clinical relevance, International journal of cardiology 130 (3) (2008) 319–325.

[44] L. A. Taber, M. Yang, W. W. Podszus, Mechanics of ventricular torsion, Journal of Biomechanics 29 (6) (1996) 745–752, cited By (since 1996):129.

[45] W. Kroon, T. Delhaas, P. Bovendeerd, T. Arts, Structure and torsion in the normal and situs inversus totalis cardiac left ventricle. ii. modeling cardiac adaptation to mechanical load, American Journal of Physiology - Heart and Circulatory Physiology 295 (1) (2008) H202–H210, cited By (since 1996):8.

[46] A. Grosberg, M. Gharib, Modeling the macro-structure of the heart: Healthy and diseased, Medical and Biological Engineering and Computing 47 (3) (2009) 301–311, cited By (since 1996):4.

[47] P. Bagnoli, N. Malagutti, D. Gastaldi, E. Marcelli, E. Lui, L. Cercenelli, M. L. Costantino, G. Plicchi, R. Fumero, Computational finite element

model of cardiac torsion, International Journal of Artificial Organs 34 (1) (2011) 44–53, cited By (since 1996):1.

[48] R. C. P. Kerckhoffs, P. H. M. Bovendeerd, J. C. S. Kotte, F. W. Prinzen, K. Smits, T. Arts, Homogeneity of cardiac contraction despite physiological asynchrony of depolarization: A model study, Annals of Biomedical Engineering 31 (5) (2003) 536–547.

[49] R. C. P. Kerckhoffs, O. P. Faris, P. H. M. Bovendeerd, F. W. Prinzen, K. Smits, E. R. McVeigh, T. Arts, Timing of depolarization and contraction in the paced canine left ventricle: Model and experiment, Journal of cardiovascular electrophysiology 14 (10 SUPPL.) (2003) S188–S195.

[50] M. P. Nash, A. V. Panfilov, Electromechanical model of excitable tissue to study reentrant cardiac arrhythmias, Progress in biophysics and molecular biology 85 (2-3) (2004) 501–522.

[51] R. C. P. Kerekhoffs, O. P. Faris, P. H. M. Bovendeerd, F. W. Prinzen, K. Smits, E. R. McVeigh, T. Arts, Electromechanics of paced left ventricle simulated by straightforward mathematical model: Comparison with experiments, American Journal of Physiology - Heart and Circulatory Physiology 289 (5 58-5) (2005) H1889–H1897.

[52] D. Nickerson, N. Smith, P. Hunter, New developments in a strongly coupled cardiac electromechanical model, Europace 7 (SUPPL. 2) (2005) S118–S127.

[53] L. Xia, M. Huo, Q. Wei, F. Liu, S. Crozier, Analysis of cardiac ventricular wall motion based on a three-dimensional electromechanical biventricular model, Physics in Medicine and Biology 50 (8) (2005) 1901–1917, cited By :35.

[54] S. A. Niederer, N. P. Smith, An improved numerical method for strong coupling of excitation and contraction models in the heart, Progress in biophysics and molecular biology 96 (1-3) (2008) 90–111.

[55] J. Aguado-Sierra, A. Krishnamurthy, C. Villongco, J. Chuang, E. Howard, M. J. Gonzales, J. Omens, D. E. Krummen, S. Narayan, R. C. P. Kerckhoffs, A. D. McCulloch, Patient-specific modeling of dyssynchronous heart failure: A case study, Progress in biophysics and molecular biology 107 (1) (2011) 147–155, cited By :23.

[56] S. J. Kovcs, D. M. McQueen, C. S. Peskin, Modelling cardiac fluid dynamics and diastolic function, Philosophical Transactions of the Royal Society A: Mathematical, Physical and Engineering Sciences 359 (1783) (2001) 1299–1314.

[57] F. Domenichini, G. Pedrizzetti, B. Baccani, Three-dimensional filling flow into a model left ventricle, Journal of Fluid Mechanics 539 (2005) 179–198.

[58] T. Doenst, K. Spiegel, M. Reik, M. Markl, J. Hennig, S. Nitzsche, F. Beyersdorf, H. Oertel, Fluid-dynamic modeling of the human left ventricle: Methodology and application to surgical ventricular reconstruction, Annals of Thoracic Surgery 87 (4) (2009) 1187–1195.

[59] P. J. Hunter, A. D. McCulloch, H. E. D. J. T. Keurs, Modelling the mechanical properties of cardiac muscle, Progress in biophysics and molecular biology 69 (2-3) (1998) 289–331.

[60] M. P. Nash, P. J. Hunter, Computational mechanics of the heart. from tissue structure to ventricular function, Journal of Elasticity 61 (1-3) (2000) 113–141.

[61] A. Krishnamurthy, C. T. Villongco, J. Chuang, L. R. Frank, V. Nigam, E. Belezzuoli, P. Stark, D. E. Krummen, S. Narayan, J. H. Omens, A. D. McCulloch, R. C. P. Kerckhoffs, Patient-specific models of cardiac biomechanics, Journal of Computational Physics 244 (2013) 4–21, cited By :14.

[62] A. Meoli, E. Cutrí, A. Krishnamurthy, G. Dubini, F. Migliavacca, T. Y. Hsia, A multiscale model for the study of cardiac biomechanics in single-ventricle surgeries: A clinical case, Interface Focus 5 (2).

[63] G. A. Holzapfel, T. C. Gasser, R. W. Ogden, A new constitutive framework for arterial wall mechanics and a comparative study of material models, Journal of Elasticity 61 (1-3) (2000) 1–48, cited By (since 1996):800.

[64] T. C. Gasser, R. W. Ogden, G. A. Holzapfel, Hyperelastic modelling of arterial layers with distributed collagen fibre orientations, Journal of the Royal Society Interface 3 (6) (2006) 15–35, cited By (since 1996):317.

[65] P. H. Backx, W. D. Gao, M. D. Azan-Backx, E. Marban, The relationship between contractile force and intracellular [ca2+] in intact rat cardiac trabeculae, Journal of General Physiology 105 (1) (1995) 1–19.

[66] D. D. Streeter, D. L. Bassett, An engineering analysis of myocardial fiber orientation in pig's left ventricle in systole, The Anatomical Record 144 (4) (1966) 503–511.

[67] P. Helm, M. F. Beg, M. I. Miller, R. L. Winslow, Measuring and mapping cardiac fiber and laminar architecture using diffusion tensor MR imaging, Vol. 1047 of Annals of the New York Academy of Sciences, 2005, cited By (since 1996):85.

[68] A. Young, B. Cowan, Evaluation of left ventricular torsion by cardiovascular magnetic resonance, Journal of Cardiovascular Magnetic Resonance 14 (1) (2012) 49.

[69] R. B. Thompson, I. Paterson, K. Chow, J. Cheng-Baron, J. M. Scott, B. T. Esch, D. B. Ennis, M. J. Haykowsky, Characterization of the relationship between systolic shear strain and early diastolic shear strain rates: insights into torsional recoil, American Journal of Physiology - Heart and Circulatory Physiology 299 (3) (2010) H898–H907.

[70] F. J. Villarreal, W. Y. W. Lew, L. K. Waldman, J. W. Covell, Transmural myocardial deformation in the ischaemic canine left ventricle, Circulation research 68 (2) (1991) 368–381, cited By :63.

[71] P. P. Sengupta, A. J. Tajik, K. Chandrasekaran, B. K. Khandheria, Twist mechanics of the left ventricle. principles and application, JACC: Cardiovascular Imaging 1 (3) (2008) 366–376, cited By :145.

[72] J. E. Hall, A. C. Guyton, Guyton and Hall textbook of medical physiology /, 12th Edition, Saunders/Elsevier,, Philadelphia, Pa. :, 2011., rev. ed. of: Textbook of medical physiology. 11th ed. 2006.

[73] M. Genet, L. C. Lee, R. Nguyen, H. Haraldsson, G. Acevedo-Bolton, Z. Zhang, L. Ge, K. Ordovas, S. Kozerke, J. M. Guccione, Distribution of normal human left ventricular myofiber stress at end diastole and end systole: A target for in silico design of heart failure treatments, Journal of applied physiology 117 (2) (2014) 142–152, cited By :1.

[74] M. Nash, Mechanics and material properties of the heart using an anatomically accurate mathematical model, Ph.D. thesis, University of Auckland (1998).

[75] J. M. Guccione, K. D. Costa, A. D. McCulloch, Finite element stress analysis of left ventricular mechanics in the beating dog heart, Journal of Biomechanics 28 (10) (1995) 1167–1177, cited By :149.

[76] W. Kroon, T. Delhaas, T. Arts, P. Bovendeerd, Computational modeling of volumetric soft tissue growth: Application to the cardiac left ventricle, Biomechanics and Modeling in Mechanobiology 8 (4) (2009) 301–309, cited By :24.

[77] K. D. Costa, Y. Takayama, A. D. McCulloch, J. W. Covell, Laminar fiber architecture and three-dimensional systolic mechanics in canine ventricular myocardium, American Journal of Physiology - Heart and Circulatory Physiology 276 (2 45-2) (1999) H595–H607, cited By :185.

[78] P. H. M. Bovendeerd, T. Arts, J. M. Huyghe, D. H. van Campen, R. S. Reneman, Dependence of local left ventricular wall mechanics on myocar-

dial fiber orientation: A model study, Journal of Biomechanics 25 (10) (1992) 1129–1140, cited By :124.

[79] A. Palit, S. K. Bhudia, T. N. Arvanitis, G. A. Turley, M. A. Williams, Computational modelling of left-ventricular diastolic mechanics: Effect of fibre orientation and right-ventricle topology, Journal of Biomechanics 48 (4) (2015) 604–612.

[80] J. Rijcken, P. H. M. Bovenoeerd, A. J. G. Schoofs, D. H. V. Campen, T. Arts, Optimization of cardiac fiber orientation for homogeneous fiber strain during ejection, Annals of Biomedical Engineering 27 (3) (1999) 289–297, cited By :71.

[81] H. Lombaert, J. M. Peyrat, P. Croisille, S. Rapacchi, L. Fanton, F. Cheriet, P. Clarysse, I. Magnin, H. Delingette, N. Ayache, Human atlas of the cardiac fiber architecture: Study on a healthy population, IEEE Transactions on Medical Imaging 31 (7) (2012) 1436–1447, cited By :37.

[82] J. Wang, D. S. Khoury, Y. Yue, G. Torre-Amione, S. F. Nagueh, Preserved left ventricular twist and circumferential deformation, but depressed longitudinal and radial deformation in patients with diastolic heart failure, European heart journal 29 (10) (2008) 1283–1289, cited By :156.

[83] L. K. Waldman, Y. C. Fung, J. W. Covell, Transmural myocardial deformation in the canine left ventricle: Normal in vivo three-dimensional finite strains, Circulation research 57 (1) (1985) 152–163, cited By :186.

[84] A. A. Young, C. M. Kramer, V. A. Ferrari, L. Axel, N. Reichek, Three-dimensional left ventricular deformation in hypertrophic cardiomyopathy, Circulation 90 (2) (1994) 854–67.

[85] T. Arts, P. H. M. Bovendeerd, F. W. Prinzen, R. S. Reneman, Relation between left ventricular cavity pressure and volume and systolic fiber stress and strain in the wall, Biophysical journal 59 (1) (1991) 93–102.

[86] T. Arts, P. Bovendeerd, T. Delhaas, F. Prinzen, Modeling the relation between cardiac pump function and myofiber mechanics, Journal of Biomechanics 36 (5) (2003) 731–736.

[87] F. Carreras, M. Ballester, S. Pujadas, R. Leta, G. Pons-Llado, Morphological and functional evidences of the helical heart from non-invasive cardiac imaging, European Journal of Cardio-thoracic Surgery 29 (SUPPL. 1) (2006) S50–S55, cited By (since 1996):8.

[88] H. J. Kim, J. H. Yoon, E. J. Lee, J. H. Oh, J. Y. Lee, S. J. Lee, J. W. Han, Normal left ventricular torsion mechanics in healthy children: Age related changes of torsion parameters are closely related to changes in heart rate, Korean Circulation Journal 45 (2) (2015) 131–140.

[89] T. G. Witkowski, J. D. Thomas, V. Delgado, E. V. Rijnsoever, A. C. T. Ng, U. Hoke, S. H. Ewe, D. Auger, K. H. Yiu, E. R. Holman, R. J. M. Klautz, M. J. Schalij, J. J. Bax, N. A. Marsan, Changes in left ventricular function after mitral valve repair for severe organic mitral regurgitation, Annals of Thoracic Surgery 93 (3) (2012) 754–760, cited By :7.

[90] E. Szymczyk, K. Wierzbowska-Drabik, J. Drozdz, M. Krzeminska-Pakula, Mitral valve regurgitation is a powerful factor of left ventricular hypertrophy, Polskie archiwum medycyny wewnetrznej 118 (9) (2008) 478–483.

[91] A. I. Veress, G. M. Raymond, G. T. Gullberg, J. B. Bassingthwaighte, Left ventricular finite element model bounded by a systemic circulation model, Journal of Biomechanical Engineering 135 (5), cited By :1.

[92] S. P. Sengupta, G. Caracciolo, C. Thompson, H. Abe, P. P. Sengupta, Early impairment of left ventricular function in patients with systemic hypertension: New insights with 2-dimensional speckle tracking echocardiography, Indian heart journal 65 (1) (2013) 48–52, cited By :5.

[93] G. A. MacGowan, D. Burkhoff, W. J. Rogers, D. Salvador, H. Azhari, P. S. Hees, J. L. Zweier, H. R. Halperin, C. O. Siu, J. A. C. Lima, J. L. Weiss,

E. P. Shapiro, Effects of afterload on regional left ventricular torsion, Cardiovascular research 31 (6) (1996) 917–925.

[94] J. Garot, O. Pascal, B. Dibold, G. Derumeaux, B. L. Gerber, J. L. Dubois-Rand, J. A. C. Lima, P. Guret, Alterations of systolic left ventricular twist after acute myocardial infarction, American Journal of Physiology - Heart and Circulatory Physiology 282 (1 51-1) (2002) H357–H362.

[95] A. N. Borg, J. L. Harrison, R. A. Argyle, S. G. Ray, Left ventricular torsion in primary chronic mitral regurgitation, Heart 94 (5) (2008) 597–603, cited By :52.

[96] J. H. Omens, Y. C. Fung, Residual strain in rat left ventricle, Circulation research 66 (1) (1990) 37–45, cited By :132.

[97] H. M. Wang, X. Y. Luo, H. Gao, R. W. Ogden, B. E. Griffith, C. Berry, T. J. Wang, A modified holzapfel-ogden law for a residually stressed finite strain model of the human left ventricle in diastole, Biomechanics and Modeling in Mechanobiology 13 (1) (2014) 99–113, cited By :6.

[98] G. A. Holzapfel, R. W. Ogden, Constitutive modelling of passive myocardium: A structurally based framework for material characterization, Philosophical Transactions of the Royal Society A: Mathematical, Physical and Engineering Sciences 367 (1902) (2009) 3445–3475, cited By :106.

[99] S. Dokos, B. H. Smaill, A. A. Young, I. J. LeGrice, Shear properties of passive ventricular myocardium, American Journal of Physiology - Heart and Circulatory Physiology 283 (6 52-6) (2002) H2650–H2659, cited By (since 1996):101.

[100] I. J. LeGrice, B. H. Smaill, L. Z. Chai, S. G. Edgar, J. B. Gavin, P. J. Hunter, Laminar structure of the heart: Ventricular myocyte arrangement and connective tissue architecture in the dog, American Journal of Physiology - Heart and Circulatory Physiology 269 (2 38-2) (1995) H571–H582, cited By :476.

[101] S. Niederer, K. Rhode, R. Razav, N. Smith, The importance of model parameters and boundary conditions in whole organ models of cardiac contraction, Lecture Notes in Computer Science (including subseries Lecture Notes in Artificial Intelligence and Lecture Notes in Bioinformatics) 5528 (2009) 348–356, cited By 0.

List of figures

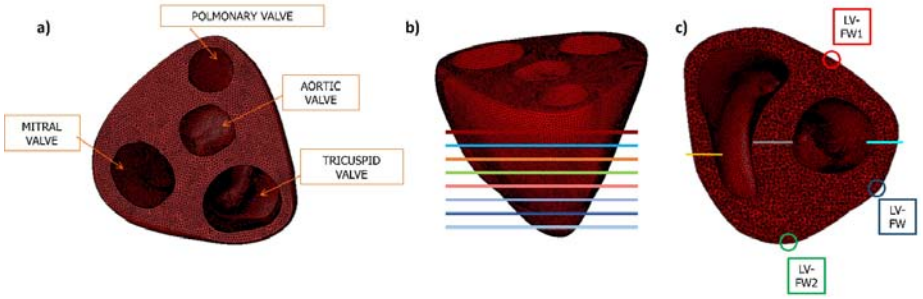

Figure 1: Geometry of the FE model with highlighted acquistion regions. *Left*: Valvular plane; *Center:* Long axis view with highlighted the cross-sections for the evaluation of the LV torsion; *Right:* Short axis view with highlighted the locations for stresses (*lines*) and cardiac torsion (*circles*) evaluation. The stress measurements were performed at the LV (*light blue*) and RV (*orange*) free wall and at the interventricular septum (*grey*), while the cardiac torsion was evaluated in LV-FW (*blue*), LV-FW1 (*red*) and LV-FW2 (*green*).

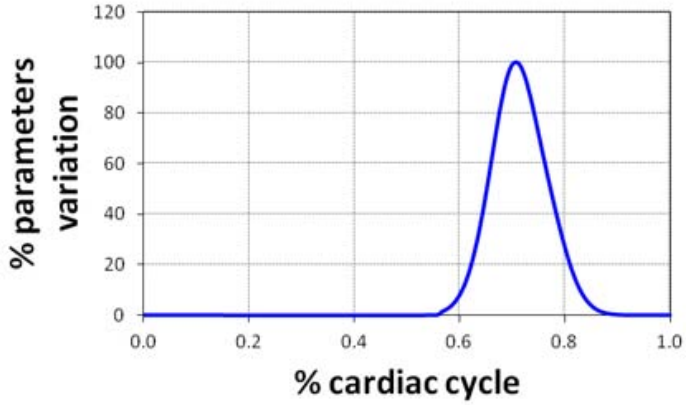

Figure 2: Percentage of fiber stiffness variation within the normalized cardiac cycle.

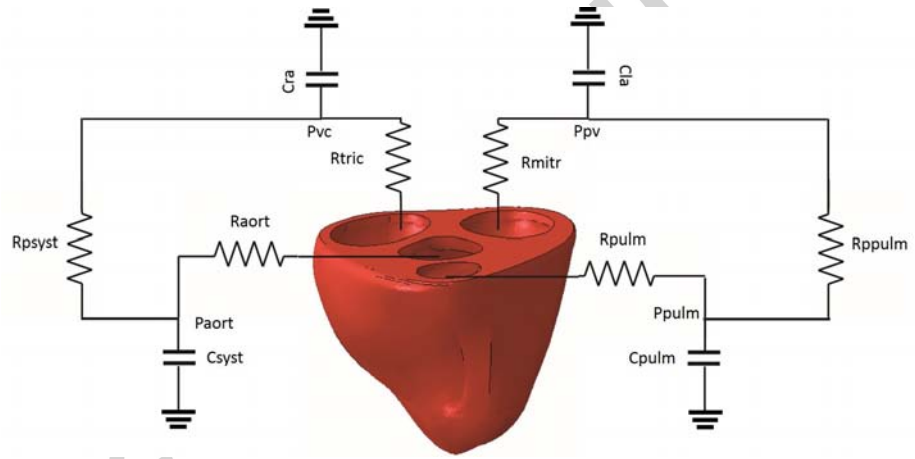

Figure 3: 3D model coupled with the LPMs of the systemic and polmonary circulations. R_{aort}: aortic valve resistance; R_{pulm}: pulmonary valve resistance; C_{syst}: systemic blood vessels compliance; C_{pulm}: pulmonary blood vessels compliance; R_{psyst}: systemic peripheral vascular resistances; R_{ppulm}: pulmonary peripheral vascular resistances; C_{la}: left atrium compliance; C_{ra}: right atrium compliance; R_{mitr}: mitral valve resistance and R_{tric}: tricuspid valve resistance.

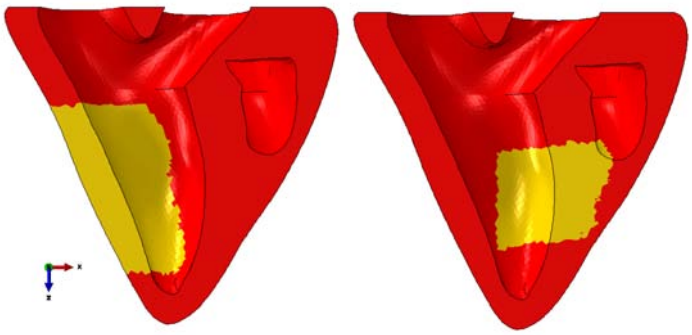

Figure 4: Locations of the infarcted regions for FW-INF (left) and SEP-FW (right).

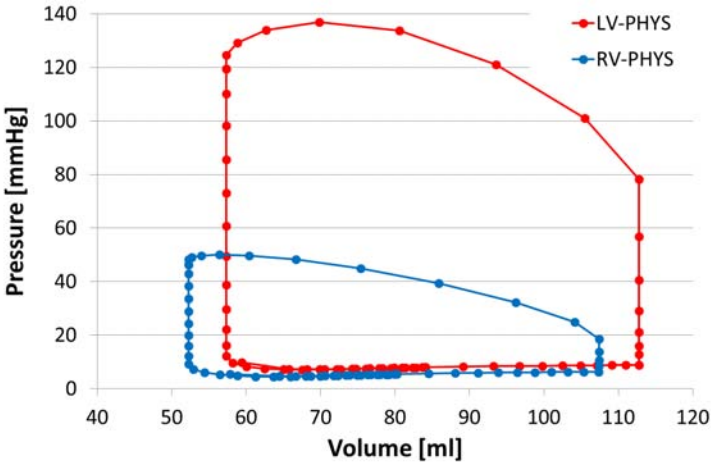

Figure 5: Physiological pressure-volume loop for the RV (blue) and the LV (red)

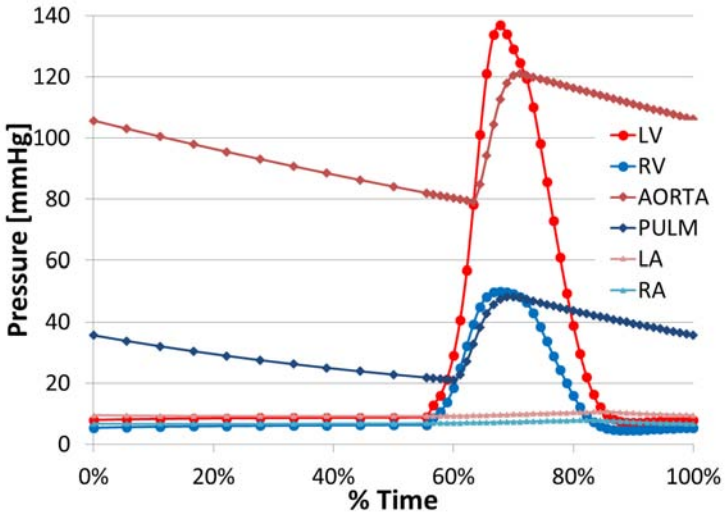

Figure 6: Physiological pressure profiles of the LV (red), the RV (blue), the LA (light red), the RA (light blue), the aorta (dark red) and the pulmonary artery (dark blue). %Time= normalized cardiac cycle duration.

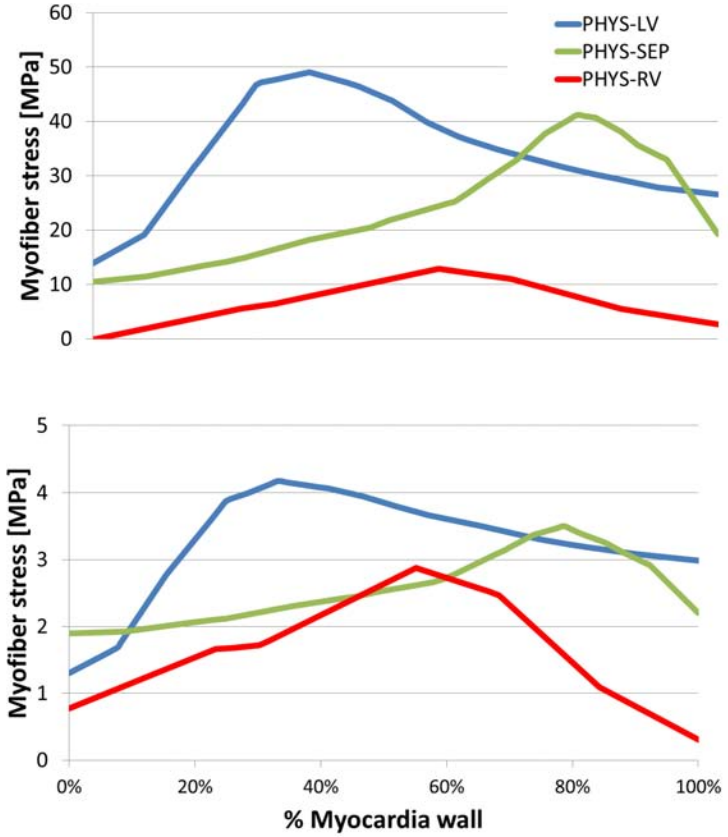

Figure 7: Physiological stress patterns at the systolic peak (*top*) and end diastolic condition (*bottom*) in three regions: LV free wall (PHYS-LV), RV free wall (PHYS-RV) and intraventricular septum (PHYS-SEP). %myocardial wall= normalized myocardial thickness where 0 refers to the endocardium while 1 to the epicardium.

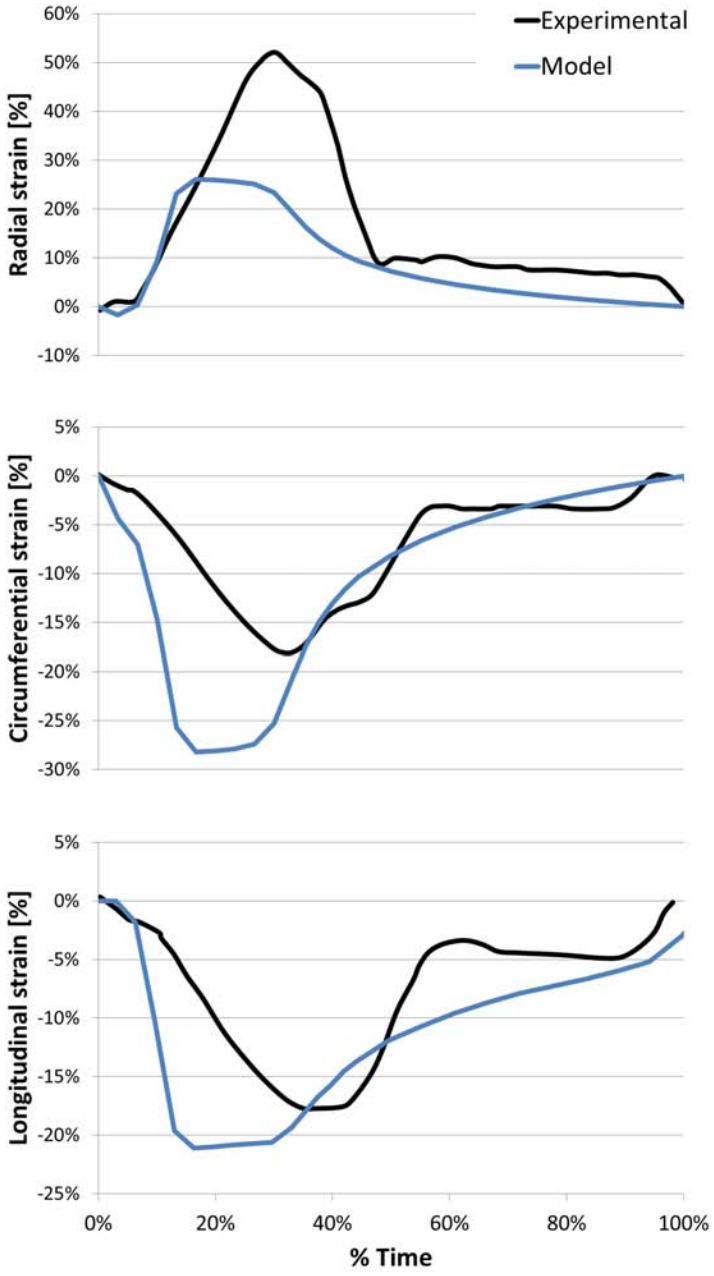

Figure 8: Physiological myofiber strains predicted by the model (*blue*) in the radial (*top*), circumferential (*middle*) and longitudinal (*bottom*) directions compared to literature experimental data (*black*) [82]. %Time= normalized cardiac cycle duration.

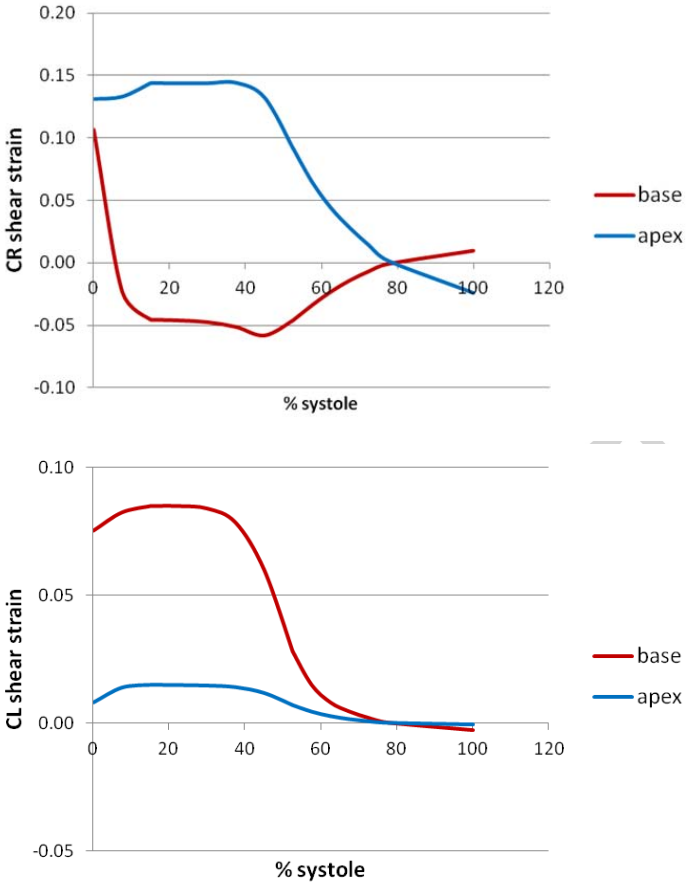

Figure 9: Circumferential-radial (CR) and circumferential-longitudinal (CL) shear strain of the basal and apical section of the left ventricle in the physiologic case.

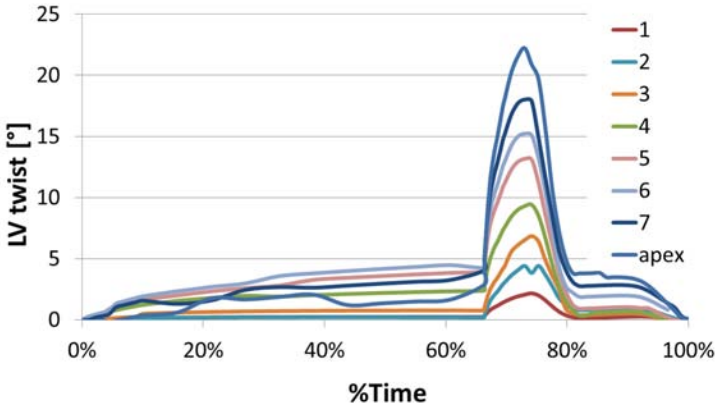

Figure 10: Physiological LV torsion for LV-FW at different cross sections with respect to the LV long axis. 1 refers to the farther section while 6 to the nearest section with respect to the apex. %Time= normalized cardiac cycle duration.

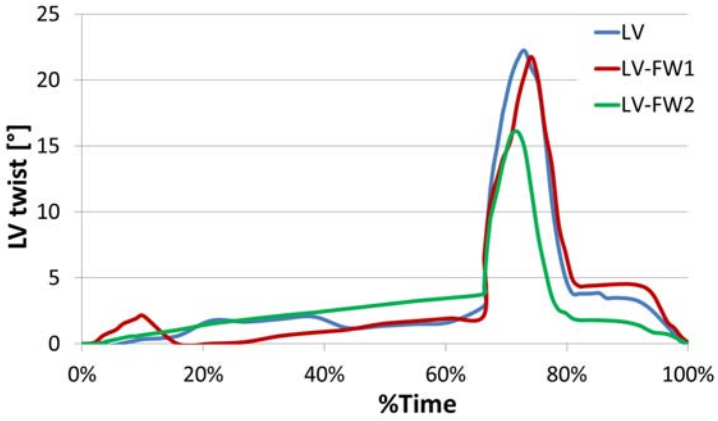

Figure 11: Physiological LV torsion for three different regions of the left ventricle: LV-FW, LV-FW1 and LV-FW2. %Time= normalized cardiac cycle duration.

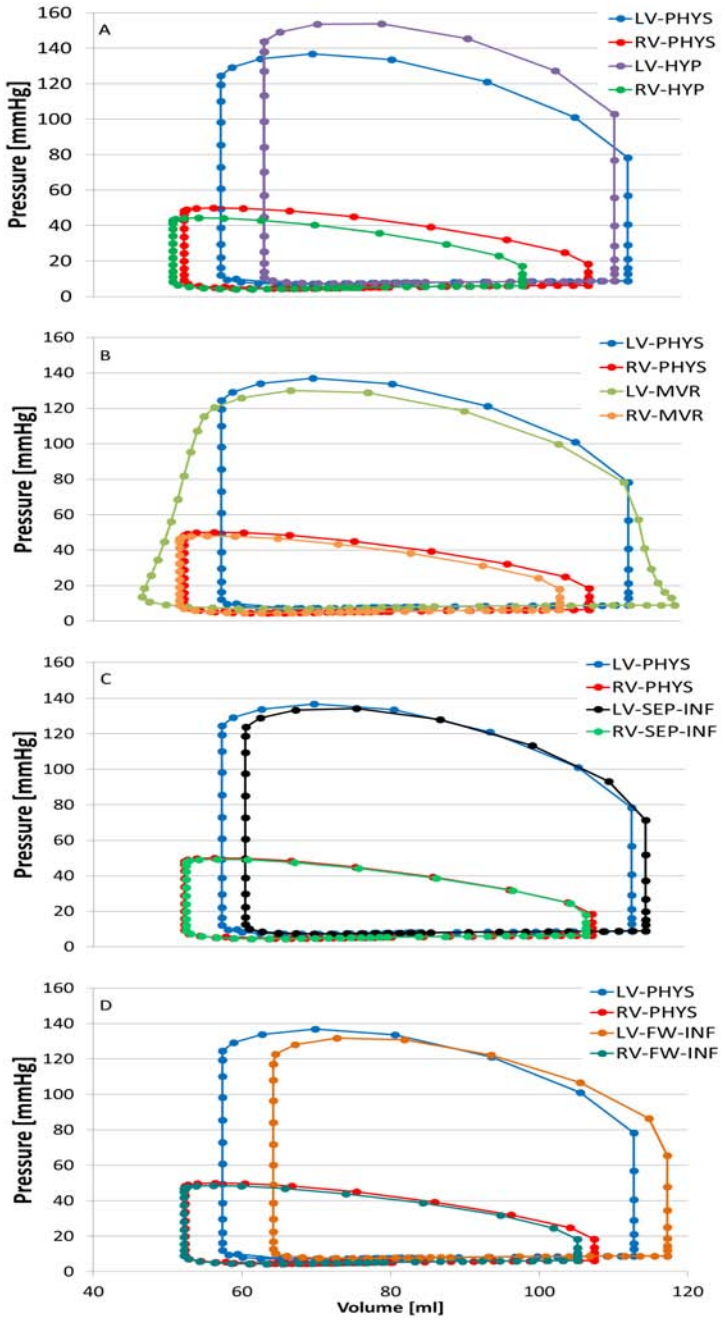

Figure 12: Comparison of the physiological PV loops (PHYS) for the LV and RV in case of (A) systemic hypertension (HYP), (B) mitral valve regurgitation (MVR), (C) infarction of the intraventricular septum (SEP-INF) and (D) the LV free wall (FW-INF).

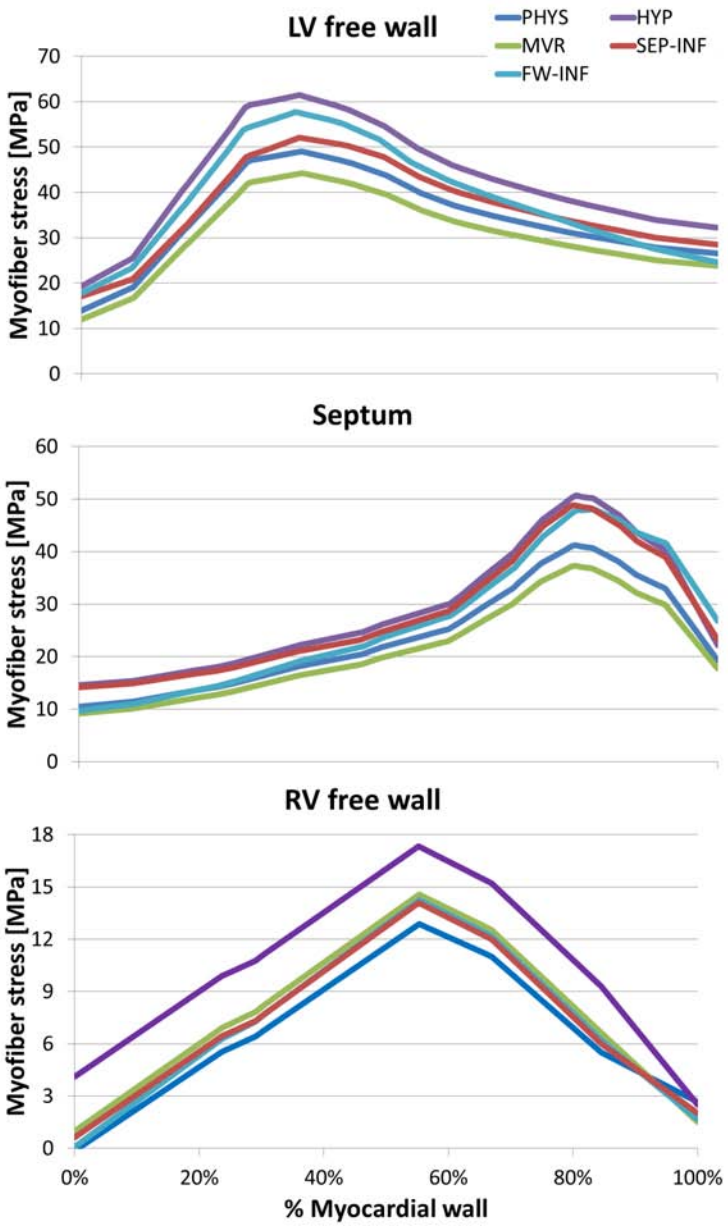

Figure 13: Myofiber stress patterns during systole evaluated in the LV free wall (*top*), interventricular septum (*middle*) and in the RV free wall (*bottom*) for the physiological case (PHYS), systemic hypertension (HYP), mitral valve regurgitation (MVR), intraventricular septum infarction (SEP-INF) and the free wall infarction (FW-INF).%myocardial wall= normalized myocardial thickness where 0 refers to the endocardium while 1 to the epicardium.

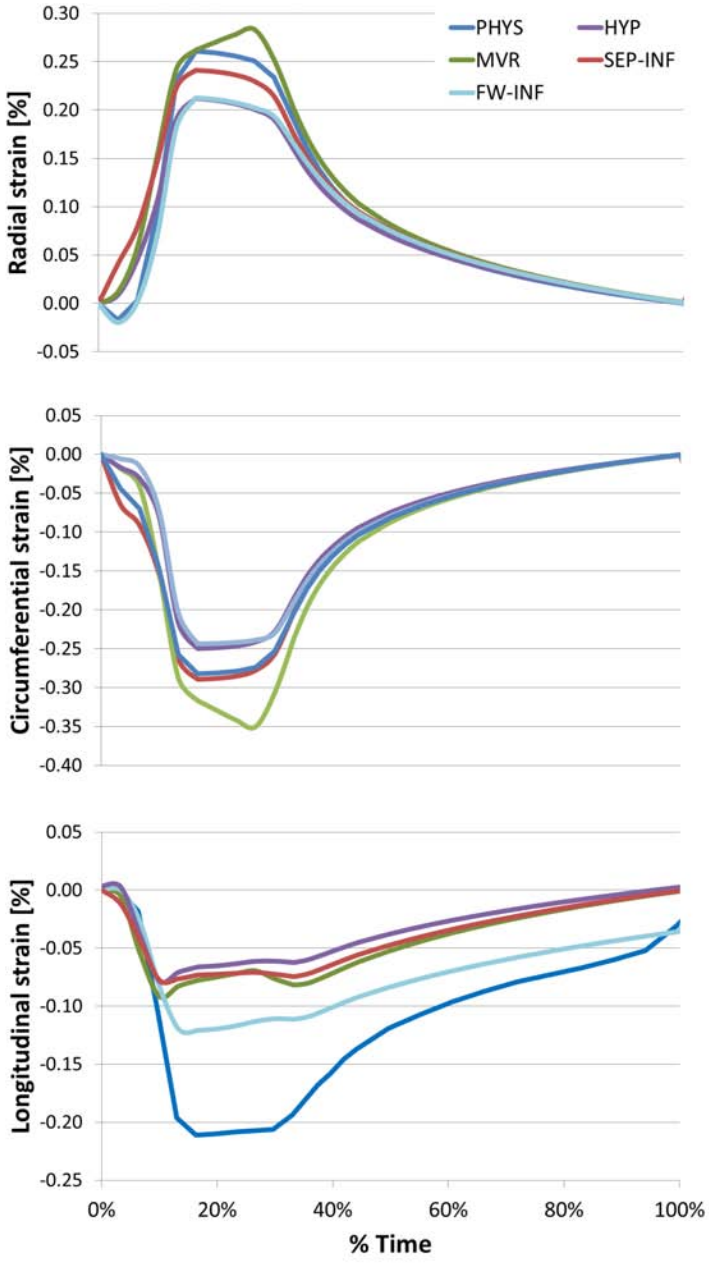

Figure 14: Comparison of the strain in the longitudinal (*top*), circumferential (*middle*) and radial (*bottom*) directions for the physiological case (PHYS), systemic hypertension (HYP), mitral valve regurgitation (MVR), intraventricular septum infarction (SEP-INF) and the free wall infarction (FW-INF). %Time= normalized cardiac cycle duration.

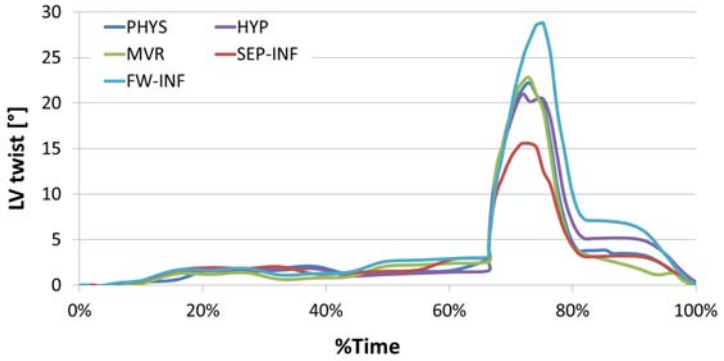

Figure 15: Comparison of the LV torsion for the physiological case (PHYS), systemic hypertension (HYP), mitral valve regurgitation (MVR), intraventricular septum infarction (SEP-INF) and the free wall infarction (FW-INF). %Time= normalized cardiac cycle duration.

List of tables

Table 1: Diastolic and systolic material parameters. c is namely the neo-Hookean parameter characterizing the matrix properties while k_1 and k_2 are a stresslike and a dimensionless parameter respectively, both referred to the fibers stiffness.

	Diastole	Systole
c [MPa]	0.0014	0.0014÷0.023
k_1 [MPa]	0.0001	0.0001÷0.045
k_2 [-]	0.01	0.01

Table 2: LPM parameter setting for the physiological condition.

	PHYS
R_{tric} $[mmHg \cdot L/min]$	0.20
C_{ra}[L/mmHg]	2.13E-02
R_{psyst} $[mmHg \cdot L/min]$	25.00
C_{syst}[L/mmHg]	1.11E-03
R_{aort} $[mmHg \cdot L/min]$	0.38
R_{mitr} $[mmHg \cdot L/min]$	0.20
C_{la}[L/mmHg]	1.33E-02
R_{ppulm} $[mmHg \cdot L/min]$	6.25
C_{pulm}[L/mmHg]	1.78E-03
R_{pulm} $[mmHg \cdot L/min]$	0.11

Table 3: Hemodynamic parameters of the RV and LV. SPP: systolic peak pressure; EDV: end diastolic volume; SV: stroke volume.

	SPP [mmHg]	EDV [ml]	SV [ml]
LV	136.9	114.6	53.55
RV	49.7	106.5	54.0